

1 **The influence of systematic structure alterations on the photophysical** 2 **properties and conjugation characteristics of asymmetric cyanine 5 dyes**

3
4 S.J. Spa,^{a, b} A.W. Hensbergen,^a S. van der Wal,^a J. Kuil,^c F.W.B. van Leeuwen^{a, b}

5
6 ^a Interventional Molecular Imaging Laboratory, Department of Radiology, Leiden University Medical Center,
7 The Netherlands.

8 ^b Laboratory of BioNanoTechnology, Wageningen, The Netherlands.

9 ^c Department of Clinical Pharmacy and Toxicology, Leiden University Medical Center, The Netherlands

10 *Corresponding Author. Albinusdreef 2, 2333 ZA Leiden, The Netherlands *Email:* F.W.B.van_Leeuwenlumc.nl
11 (F.W.B. van Leeuwen)

12

13 Keywords: Cyanine dyes, Protein conjugation, Far-red fluorescence, Fluorescence-guided surgery,
14 Molecular imaging

15

16 **Abstract**

17 The light spectrum above 650 nm allows for good tissue penetration depths, far-red and near-
18 infrared fluorescent dyes are therefore popular fluorophores applied in (bio)medical diagnostics,
19 including image-guided surgery. However, near-infrared fluorescent dyes often suffer from
20 instability and limited brightness, two important features that, together with the labelling efficiency
21 (*e.g.*, non- one- or di-conjugated products) and serum-dye interactions are key elements that drive
22 *in vivo* characteristics. Due to the fact that stability and brightness of far-red fluorophores are often
23 superior over near-infrared dyes, interest in the use of dyes such as Cy5 is increasing. As there are
24 clear indications that the influence of the chemical structure on the (photo)physical properties of a
25 dye is dye-structure-dependent, the (photo)physical properties of ten structural variants of
26 asymmetrical Cy5-(R₁)R₂-(R₃)COOH (R representing the varied substituents) were extensively studied,
27 While stacking in solution was not induced in most of the Cy5 far-red fluorophores, multimers and

28 stacking characteristics were observed in protein conjugates. And although all dye variants were
29 shown to be stable towards photobleaching, clear differences in brightness and serum interactions
30 were found. Combined, these findings indicate that the chemical substituents prominently influence
31 the photophysical properties of Cy5 dyes, a feature that should be considered when using
32 fluorescent dyes in future tracer development.

33

34 **1. Introduction**

35 Fluorescent dye-based guidance during surgical interventions is being recognised as an improvement
36 in the accuracy of clinical care [1–3]. In clinical trials, fluorescence imaging has been used as a sole
37 modality or in a bimodal/hybrid form, wherein it extends the field of nuclear medicine [4]. While
38 fluorescence emissions across the light spectrum have been used for image guided surgery [2],
39 emphasis lies on the use of dyes emitting in the far-red ($650 \text{ nm} < \lambda_{\text{em}} < 750 \text{ nm}$) or near-infrared
40 (NIR) region ($\lambda_{\text{em}} \geq 750 \text{ nm}$)[5]. This theoretical preference can be attributed to the enhanced
41 penetration depths and limited auto-fluorescence in at these wavelengths.

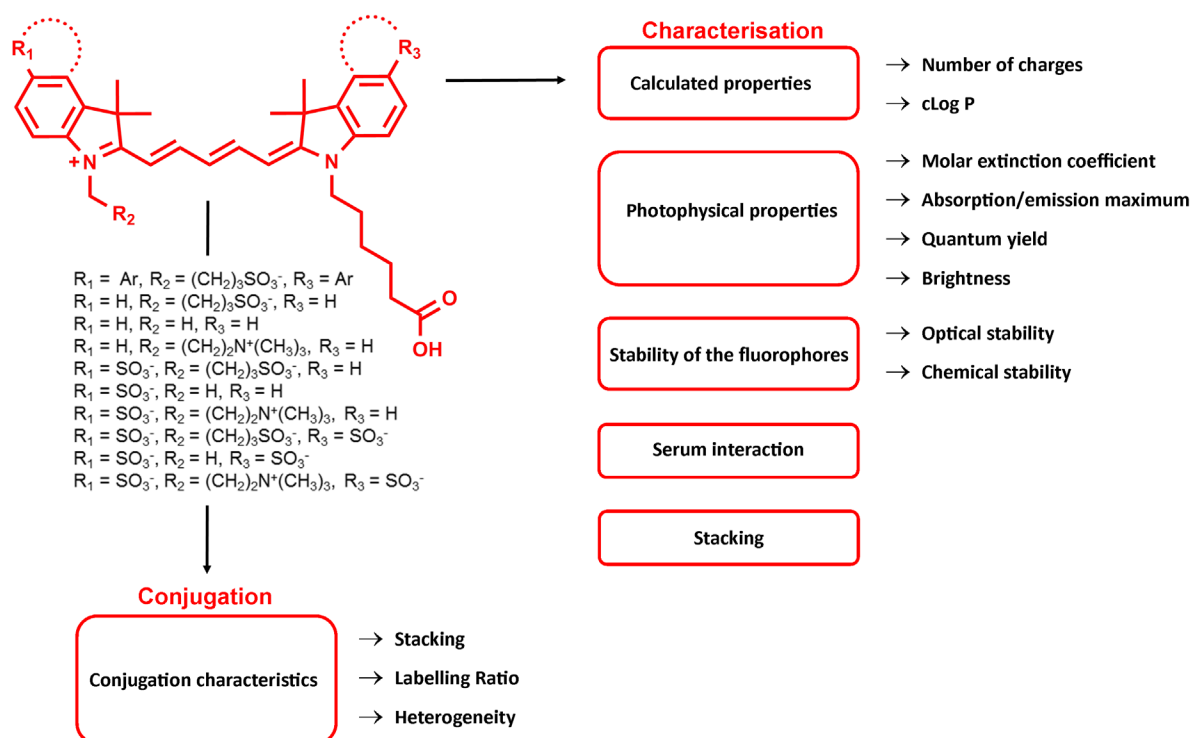
42 Unfortunately, the dye chemistry, stability and/or photophysical properties of near-infrared
43 dyes are limited compared to dyes emitting at lower wavelengths. For example, the most commonly
44 applied near-infrared dye indocyanine green (**ICG**) is prone to stack/aggregate from aqueous
45 solutions and has a low quantum yield ($Q_{\text{F}} = 0.3\%$ in H_2O)[6]. More experimental dyes such as IRdye
46 800CW also have a low quantum yield ($Q_{\text{F}} = 3.4\%$ in H_2O)[7] and have been shown to be chemically
47 unstable with respect to endogenous nucleophiles [8]. These limitations have boosted the interest in
48 far-red dyes. For instance, methylene blue (**MB**), a clinically applied dye with a weak far-red
49 fluorescence emission ($Q_{\text{F}} = 3\%$ in H_2O) has been applied in humans to image ureters [9], parathyroid
50 glands [10], and bile ducts [11], despite the FDA warning against its use [12]. As an alternative, the
51 Cy5 family provides relatively bright ($\sim 3 \cdot 10^4 \text{ M}^{-1} \cdot \text{cm}^{-1}$, $Q_{\text{F}} \approx 20\%$ in H_2O)[13] far-red fluorophores and
52 encompasses many structural variations. A prime example of a Cy5-based imaging agent in clinical
53 use is found in GE-137 (now EM-137), a Cyanine 5 (Cy5)-labelled c-Met-targeting peptide that was

54 effectively used for identification of colorectal polyps in humans [14]. Furthermore, the Cy5-
55 containing nanoparticles ¹²⁴I- cRGDY-PEG-C have been used to target metastatic melanoma [15].

56 To convert Cy5-dyes into imaging agents of value for fluorescence-guided surgery, these
57 dyes have to be conjugated to targeting vectors. When a targeting vector has multiple conjugation
58 sites, *e.g.* a protein, labelling may not be straightforward. A ratio of one dye per targeting vector is
59 generally aimed at, but the final product often consists of, *e.g.*, a mixture of none-, one-, di-, and/or
60 tri-dye conjugated imaging agents. In case multiple dyes are located on a single targeting vector, the
61 occurrence of dye-stacking or Förster Resonance Energy Transfer (FRET) between the dyes can cause
62 luminescence quenching, a feature that reduces the brightness of the imaging agent [8].

63 Conjugation of imaging labels, and especially an excess thereof, may also negatively
64 influence the binding specificity and pharmacokinetics of a targeting vector. Dependent on the size
65 of the targeting vector, the scale of these effects varies [16], being most prominent when relatively
66 small peptides are used [14,17]. Nevertheless, this effect is also reported for larger proteins, *e.g.*,
67 mAb conjugates [18]. When dyes express an affinity for serum proteins such as human serum
68 albumin, *e.g.*, **ICG** and Cy5-(Ar)SO₃-(Ar)SO₃ [19–21], this may further effect the tracer
69 pharmacokinetics.

70 In order to determine the influence of the structure of a florescent dye on its utility as an
71 imaging label, ten Cy5 analogues were synthesised and compared with the reference compound **MB**.
72 By alternating the aromatic (R₁ and R₃) and alkyl substituents (R₂), molecular variations on Cy5-
73 (R₁)R₂-(R₃)COOH were systematically evaluated for their photophysical properties, chemical- and
74 photo-stability, serum protein interaction, dye–dye stacking tendencies, and conjugation efficiency
75 (Figure 1).



76

77 **Figure 1.** Overview of the subjects and fluorophore properties investigated and discussed throughout the
78 article.

79

80 **2. Experimental**

81 **2.1. Materials and reagents**

82 For the synthesis of the fluorophores (Compound **1-21**), cLog P calculations, and information on the
83 materials used, please refer to the Supporting information (SI). The electron density modelling is
84 reported in Ref [22]

85

86 **2.2 Ubiquitin Labelling (compound 22–30)**

87 Stock solutions of the NHS-activated fluorophores (**12–21**, see SI) were prepared in DMSO and the
88 percentage of activated dye was determined by HPLC (see also SI ‘NHS activation’). Subsequently,
89 Ubiquitin (16 nmol) was dissolved in 500 μ L of phosphate buffer (0.1 M, pH 8.4, 2.67 g HNa_2PO_4 +
90 0.14 g H_2NaPO_4 in 200 μ L H_2O). Appropriate amounts of the fluorophore stock solution were added,
91 ensuring that each sample contained 3 equivalents activated dye (50 nmol, 100 μ M final

92 concentration) and that the DMSO content in the final solution was < 10%. The mixtures were
93 shaken at room temperature for 6.5 h and the labelled Ubiquitin was washed with PBS by filtration
94 over a 3K Amicon® filter subsequently. When the filtrate was no longer blue, the residue was
95 collected in 100 µL PBS.

96 Dye–Ubiquitin conjugates were analysed by mass spectrometry and absorption
97 measurements using a NanoDrop. To determine the average labelling ratio, the dye concentration
98 was calculated from absorption measurements in DMSO around 650 nm (Table 1) and the obtained
99 values were then divided by the known protein concentration (0.16 mM). For compound **30**
100 significant precipitation was observed after the reaction, therefore the protein content in this
101 sample also was determined by absorption ($\epsilon_{280} = 1490 \text{ M}^{-1}\cdot\text{cm}^{-1}$, calculated from the amino acid
102 sequence) [23]. Since Cy5 also shows absorbance at this wavelength, a correction was made by
103 measuring the absorbance of free dye at this concentration and subtracting it from the absorbance
104 value measure for the dye containing Ubiquitin.

105

106 **2.3 Photophysical properties**

107 *2.3.1. Molar extinction coefficient (ϵ) of compound 1–11*

108 To obtain a 4 mM stock solution of **MB (1)**, 3.2 mg Methylene blue hydrate (Fisher Scientific) was
109 dissolved in 4 mM ethylene carbonate in DMSO- d_6 (1500 µL) and the exact concentration was
110 determined by NMR using ethylene carbonate as internal standard [8].

111 To allow for absorption measurements, the 4 mM stock solutions of the dyes in DMSO- d_6 (**1-**
112 **11**, for details, see SI) were diluted to 100 µM in DMSO, H₂O or PBS. From the 100 µM concentration,
113 50 µM and 5 µM concentrations were made from which further two-fold dilution in the same
114 medium followed to obtain a final concentration range of 100, 50, 25, 12.5, 5, 2.5, 1.2, 0.6, and 0.3
115 µM, respectively. Absorption spectra were measured using 1 mL disposable plastic cuvettes ($l = 1$
116 cm; Brand, Germany) for concentrations $\leq 5 \mu\text{M}$, quartz cuvettes ($l = 0.1 \text{ cm}$; Hellma standard cell,
117 Macro) for 12, 25, and 50 µM concentrations, and two glass microscopy slides held together with a

118 0.14 mm thick PET plastic spacer for the 100 μ M concentration to keep the signal below 1.5 AU.
119 Optical density was measured 10 minutes after preparation and the plotted absorbance was
120 normalised for cuvette path length and concentration. The ϵ was then determined by applying a
121 linear regression coefficient.

122

123 2.3.2. Absorbance spectra of the labelled Ubiquitin (**22–30**)

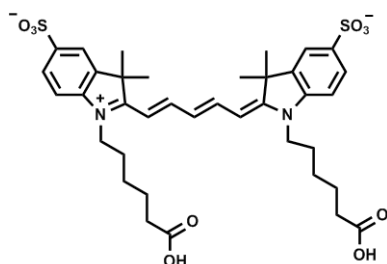
124 The Ubiquitin solutions collected after synthesis (for synthesis procedures see SI) were diluted 100 x
125 in PBS and the absorbance spectra were measured using NanoDrop. Subsequently, the obtained
126 spectra were normalised for dye concentration.

127

128 2.3.3. Quantum yield and emission maximum determination of compound **1–11** and **22–30**

129 Fluorescence spectra were measured at $\lambda_{\text{ex}} = 606$ nm for compounds **3–11** and the Ubiquitin
130 conjugates **22–30**, and $\lambda_{\text{ex}} = 620$ nm for **1–2**, using 1 cm disposable plastic 4.5 mL cuvettes (Kartell,
131 Germany). 3 mL of 0.5 μ M dye was prepared in PBS (**1–11**, **22–30**) by first preparing 100 μ M
132 solutions in PBS from the DMSO- d_6 dye stock (**1–9** and **MB** solutions) or from dilutions of the
133 Ubiquitin conjugates (**22–30**) (see SI for synthesis). To determine the quantum yield, the absorbance
134 at $\lambda = 606$ (compounds **3–11** and **22–30**) or $\lambda = 620$ nm (compound **1–2**) of 0.5 μ M and 0.25 μ M were
135 measured and correlated with the integrated fluorescent emission. The regression coefficient of the
136 resulting plot for the unknown dyes was then compared to the regression coefficient of Cy5-
137 (SO_3)COOH-(SO_3)COOH (Figure 2), which has a known quantum yield ($Q_F = 27\%$) [13].

138



139

140 **Figure 2.** Chemical structure of the reference compound applied for the quantum yield determination; Cy5-
141 (SO₃)COOH-(SO₃)COOH.

142

143 **2.4 Stability**

144 *2.4.1 Chemical stability of compound 1–11 towards glutathione*

145 Solutions of 0.25 mM dye (from DMSO-d₆ NMR solutions) and 0.5 mM glutathione in 4-(2-
146 hydroxyethyl)-1-piperazine-ethanesulfonic acid buffer (HEPES, 0.1 M, pH 7.4) were freshly made.
147 Prior to the addition of glutathione to the HEPES buffer, nitrogen was bubbled through the HEPES
148 buffer to remove oxygen and reduce the rate of disulfide formation of glutathione. The solutions
149 were immediately put into the sample manager (37 °C) of a Waters Acquity UPLC-MS system
150 equipped with an Acquity UPLC photodiode array detector, an SQ Detector mass spectrometer and a
151 Waters BEH C18 130 Å 1.7 μm (100 × 2.1 mm) column (flow rate: 0.5 mL/min). Analysis was
152 performed every 30 minutes using a gradient of 0.05% TFA in H₂O/0.04% TFA in CH₃CN 95:5 to 0.05%
153 TFA in H₂O/0.04% TFA in CH₃CN 5:95 in 5.44 minutes. The stability of the dyes was calculated relative
154 to the integration of the chromatogram at t = 0 h.

155

156 *2.4.2 Optical stability of compound 1–11*

157 For the optical stability measurements, a prototype Karl Storz camera setup (KARL STORZ Endoskope
158 GmbH & Co. KG, Tuttlingen, Germany) was applied. This camera setup included an IMAGE1 S H3-Z FI
159 Three-Chip FULL HD camera head equipped with a 0° laparoscope in combination with an IMAGE 1 S
160 CONNECT module, an IMAGE 1 S H3-LINK link module and a Cy5-modified D-light C light source (590-
161 680 nm emission). A standard eyepiece adaptor containing a filter that passes through light between
162 640–720 nm (Cat no. 20100034; KARL STORZ Endoskope GmbH & Co. KG) was placed between the
163 camera and the laparoscope to image the Cy5 fluorescence.

164 From the DMSO-d₆ dye stock solutions (see synthesis in SI) 100 μM solutions in PBS were
165 prepared. Subsequently, from the 100 μM solutions, 3.0 mL of 1 μM solutions were prepared in 4.5

166 mL disposable cuvettes (Kartell, Germany). The cuvettes were placed in front of the prototype Karl
167 Storz camera and illuminated at maximum intensity for 30 minutes. At 5-minute intervals the
168 fluorescence was measured with $\lambda_{ex} = 602$ nm. The reduction in fluorescence intensity was plotted
169 and normalised relative to the fluorescence intensity obtained at $t = 0$ minutes.

170

171 **2.5 Serum protein interaction**

172 Serum protein binding was assayed using the single-use Rapid Equilibrium Dialysis (RED) plate kit
173 with an 8 kD MWCO (Pierce, Thermo Scientific). Serum (300 μ L, fetal bovine serum, heat inactivated)
174 was placed into the dialysis chamber and phosphate buffer (500 μ L, 100 mM phosphate and 150 mM
175 NaCl, pH = 7.2) was placed into the reservoir chamber. The dyes were added from a DMSO stock
176 (100 μ M, 3 μ L) to the dialysis chamber ($n = 2$) and in duplicate samples ($n = 2$) to the reservoir
177 chamber. The plate was subsequently closed using sealing tape and incubated at room temperature
178 on a rocking shaker for 18 h, after which 100 μ L aliquots were withdrawn from both chambers for
179 each dye. 100 μ L phosphate buffer was then added to the aliquots containing serum, and 100 μ L
180 serum was added to the aliquots containing phosphate buffer. All aliquots were transferred to a
181 white 96 well plate (Greiner Lumitrac 600) and fluorescence was quantified at $\lambda_{ex} = 620$ nm using a
182 PerkinElmer LS 55 fluorometer (equipped with a red-sensitive detector and a plate-reader
183 attachment). Serum protein binding percentages were calculated using the manufacturer's protocol
184 (eq. 1):

$$\%_{bound} = \left(100 - \frac{[buffer\ chamber]}{[serum\ chamber]} \right) \cdot 100 \quad \text{eq. 1}$$

185

186 **2.6 Stacking behaviour of compound 1–11 in different solvents**

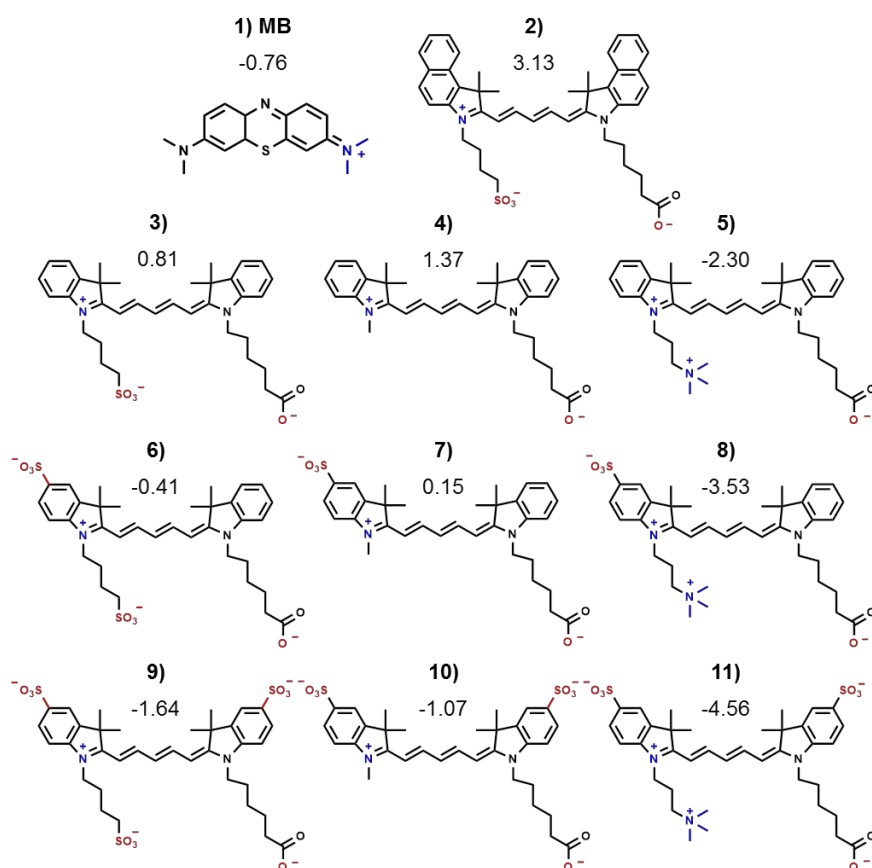
187 To determine the stacking behaviour of the dyes (**1–11**) in DMSO, H₂O or PBS, the same dilutions and
188 absorbance measurements were performed as described for measuring the molar extinction
189 coefficient (chapter 2.3.1). For a more detailed description please refer to Ref [22].

190 **3. Results and Discussion**

191 **3.1 Chemical properties**

192 The number of charges, and calculated Log P (cLog P) values of the investigated fluorophores are
193 given in Figure 3. Overall, the calculated net charge decreased with increasing number of sulfonate
194 moieties on the aromatic ring, which also resulted in decreasing cLog P values. The highest cLog P
195 value was, as expected, calculated for compound **2** due to the presence of additional benzene rings.
196 The lowest cLog P value was found for compound **11**, as a result of the high total number of charges
197 (5). The cLog P value of **MB (1)** was most similar to the cLog P value calculated for compound **6**.

198



199

200 **Figure 3.** The cLog P values of the compounds **1–11**. In the compound structures the positively charged groups
201 are indicated in blue and negatively charged groups are indicated in red.

202

203 **3.2 Photophysical properties**

204 The molar extinction coefficient (ϵ) was calculated *via* the regression coefficient between the
205 concentration and the absorbance determined from a linear concentration range between 0.3–5 μM
206 in DMSO, H_2O , and PBS. In DMSO, except for compounds **2**, **4** ($\epsilon \approx 185.000 \text{ M}^{-1}\text{cm}^{-1}$) and **MB (1)**, $\epsilon =$
207 $84.000 \text{ M}^{-1}\text{cm}^{-1}$), all dyes had $\epsilon > 200.000 \text{ M}^{-1}\text{cm}^{-1}$. The ϵ determined for **MB** in DMSO was in line with
208 the literature, which reports values between 70.000 and $95.000 \text{ M}^{-1}\text{cm}^{-1}$ [24,25]. For compounds **3–8**
209 the ϵ decreased with about 25% when changing the solvent from DMSO to H_2O or PBS. A more
210 substantial decrease (37%) was observed for the more lipophilic compound **2**. Remarkably, for the
211 more soluble compounds with two aromatic sulfonates (**9–11**) the change in solvent resulted in a
212 10% increase in the ϵ and gave extinction coefficients of 242.000 , 220.000 and $231.000 \text{ M}^{-1}\text{cm}^{-1}$ in
213 PBS respectively (Table 1).

214 The absorption/emission maxima of the Cy5 fluorophores (**2–11**) observed in DMSO had
215 Stokes shifts of about 20 nm (Table 1) while **MB (1)** had a Stokes shift of 16 nm. Changing the solvent
216 from DMSO towards H_2O or PBS caused a hypsochromic shift in the absorption/emission maximum
217 of 10 nm for **2–11** and only a minor shift (5 nm) for **MB**. Comparison of the absorption/emission
218 maxima (Table 1) with the structure of the dyes (Figure 3), revealed that all compounds with a
219 sulfonate on both aromatic rings (**9–11**) displayed a slight bathochromic shift of around 5 nm in their
220 maxima. This bathochromic shift has also been reported for other Cy5-fluorophores [26]. This effect
221 was, however, not observed when no or just one aromatic sulfonate was present at this location
222 (*e.g.*, **9** vs **3** and **6**, Table 1).

223 In practice, the environment of the fluorophores will be aqueous, hence the quantum yields
224 measurements were performed in PBS and related to that of $\text{Cy5}-(\text{SO}_3)\text{COOH}-(\text{SO}_3)\text{COOH}$ ($\Phi_f = 27\%$)
225 [13]. In line with the above-presented molar extinction coefficients, the quantum yields of
226 compounds **9**, **10**, and **11** were also the highest (23%) from the series; the other Cy5-dye derivatives
227 displayed quantum yields around 13% or lower (Table 1). In contrast, **MB** yielded a quantum yield of
228 merely 3%. It is interesting to note that the quantum yields did not alter significantly upon changing
229 the alkyl substituent (*e.g.*, **3** vs **4** vs **5**, Table 1), or changing the number of aromatic sulfonates from

230 0 to 1 (e.g., **3** vs **6**). As Fisher *et al.* suggested [27], a clear trend between the structure of dyes and
 231 the quantum yield seems to be missing.

232

233 **Table 1.** Photophysical properties of compound **1–11**, including the quantum yields of **22–30**.

Dye	ϵ in DMSO ^a (M ⁻¹ ·cm ⁻¹)	ϵ in water ^a (M ⁻¹ ·cm ⁻¹)	ϵ in PBS ^a (M ⁻¹ ·cm ⁻¹)	$\lambda_{ex}/\lambda_{em}$ in DMSO (Stokes shift; nm)	$\lambda_{ex}/\lambda_{em}$ in H ₂ O and PBS (Stokes shift; nm)	Φ_F in PBS ^b Non- conjugated	Φ_F in PBS ^b Conjugated (22–30)
MB (1)	84 · 10 ³	77 · 10 ³	71 · 10 ³	670/686 (16)	665/679 (14)	3%	n.a. ^c
2	181 · 10 ³	113 · 10 ³	112 · 10 ³	688/710 (22)	678/695 (17)	10%	n.a. ^c
3	200 · 10 ³	199 · 10 ³	203 · 10 ³	655/671 (16)	643/659 (16)	14%	5%
4	188 · 10 ³	176 · 10 ³	174 · 10 ³	647/667 (20)	640/656 (16)	13%	10%
5	218 · 10 ³	193 · 10 ³	193 · 10 ³	658/677 (19)	638/658 (20)	13%	12%
6	228 · 10 ³	206 · 10 ³	206 · 10 ³	655/675 (20)	643/660 (17)	13%	9%
7	238 · 10 ³	176 · 10 ³	212 · 10 ³	653/672 (19)	642/658 (16)	13%	3%
8	200 · 10 ³	146 · 10 ³	149 · 10 ³	647/673 (26)	637/657 (20)	9%	14%
9	219 · 10 ³	245 · 10 ³	242 · 10 ³	660/679 (19)	648/664 (16)	22%	21%
10	204 · 10 ³	233 · 10 ³	220 · 10 ³	658/677 (19)	646/662 (16)	23%	14%
11	209.0 · 10 ³	223 · 10 ³	231 · 10 ³	659/677 (18)	645/661 (16)	23%	20%

234 a) Fresh dilutions from the DMSO stock were made and measured within 2 hours

235 b) Relative quantum yield, compared to Cy5-(SO₃)COOH-(SO₃)COOH ($\Phi_F = 27\%$)[13]

236 c) Labelling was not successful

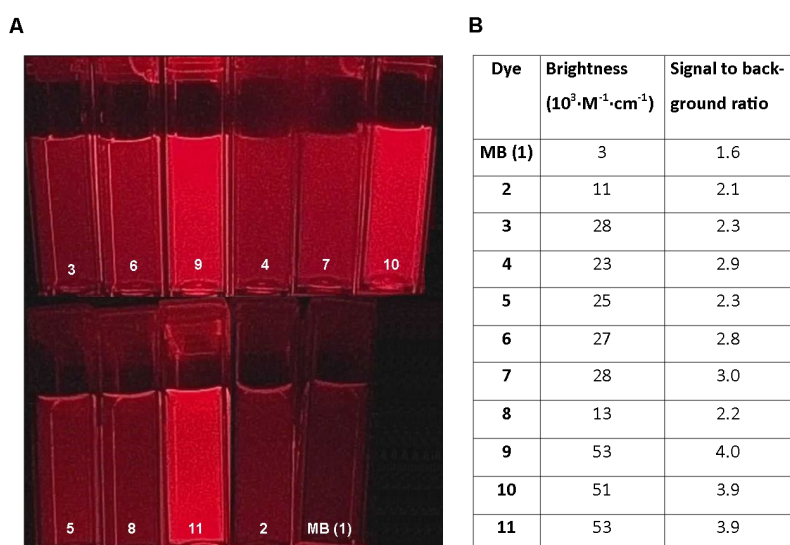
237 With ϵ for molar extinction coefficient, $\lambda_{ex}/\lambda_{em}$ for excitation/emission wavelength, Φ_F for quantum yield and
 238 n.a. for not applicable.

239

240 Although emphasis is generally placed on the molar extinction coefficient or quantum yield
 241 individually, the combination of both properties, *i.e.*, the brightness (quantum yield x molar
 242 extinction coefficient)[28], often gives more insight in the optical capability of the fluorophores. This
 243 difference also becomes apparent from Figure 4, where all 11 fluorophores are imaged by a
 244 prototype Karl Storz camera setup ($\lambda_{ex} = 590–680$ nm, data collection between 640–750 nm). For
 245 proper *in vivo* visualisation, a signal-to-background ratio (e.g., tumour to muscle) of at least 2 is
 246 required [29]. On the basis of the signal-to-background ratio calculated from Figure 4, one can

247 deduct that a brightness $> 1 \cdot 10^4 \text{ M}^{-1} \cdot \text{cm}^{-1}$ is required to achieve a signal to background ration > 2 .
 248 With a brightness of $3 \cdot 10^3 \text{ M}^{-1} \cdot \text{cm}^{-1}$ and a signal to background ration of 1.6, **MB** fluorescence was
 249 considered too weak to be detected accurately (Figure 4B). Since fluorescence imaging of **MB** has
 250 already been used in clinical trials, this finding underlines the medical potential of the relatively
 251 bright Cy5 dyes [30].

252



253

254

255 **Figure 4.** Brightness of the fluorophores in PBS ($1 \mu\text{M}$) measured by Storz camera (A) or calculated (B). From
 256 the image (A) the corresponding signal to background ratios were calculated (B). Overall, the fluorophores
 257 with two aromatic sulfonates (**9–11**) emit the brightest fluorescence, while **MB** is hardly visible at all (signal to
 258 background ratio < 2).

259

260 Figure 4 indicates that the fluorophores with two aromatic sulfonates (**9–11**) possess the
 261 best optical properties. It is known that electron-withdrawing groups, *e.g.*, sulfonates, substituted on
 262 the aromatic ring, increase the brightness of such fluorophores [31]. Interestingly, despite their
 263 match in brightness, Spartan calculations revealed differences in the theoretical electron densities
 264 (Figure 2 in Ref [22], please refer to Ref [22] for further details). Hence, in line with the report by
 265 Levitus *et al.*, [32] the positive effect of aromatic sulfonates on the optical properties might not solely

266 lie in the electrostatic withdrawing capacity. According to the combined data in Table 1 and Figure 2
267 in Ref [22], the concept of reinforced conformational stability seems to offer a more probable explanation
268 for the sulfonate induced increase in fluorescence brightness; *cis-trans* photoisomerisations of the
269 central methine bridge influences the fluorescence brightness [33]. In the ground state, the main
270 conformation of the Cy5 dyes is the *trans*-conformation [32]. However, when excited, the methine
271 bridge can rotate around its C–C bonds, twisting towards the *cis*-conformation [32,34]. In the *cis*-
272 conformation, the most probable route towards the ground state is *via* non-luminescent internal
273 conversion due to the high overlap in the vibronic wave functions (Frank-Condon factor) [26]. It has
274 been speculated that sulfonation of the aromatic rings increases the stability of the *trans*-
275 conformation, thereby reducing the rate of *cis-trans* photoisomerisation [32,34] and increasing the
276 fluorescence brightness.

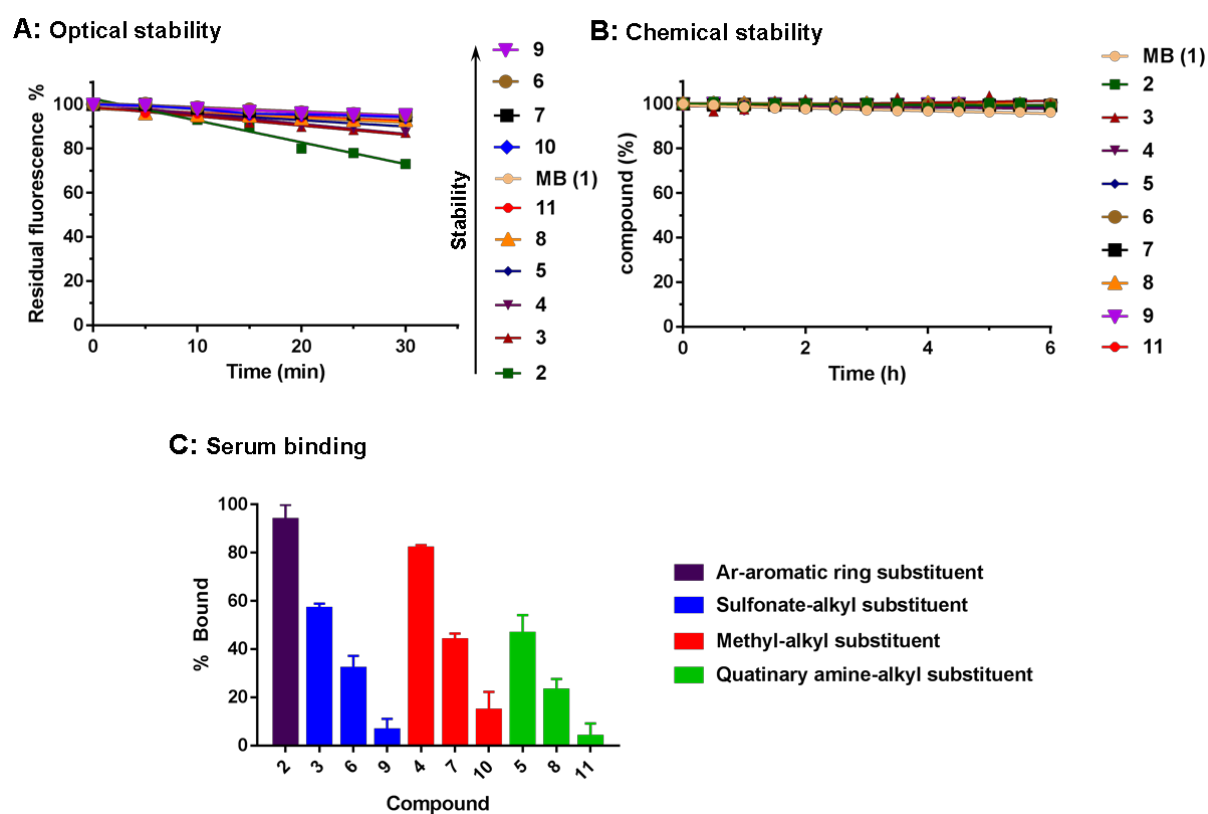
277

278 **3.3 Stability of the fluorophores**

279 As the fluorophores **2–11** were synthesised with a future use in image-guided surgery in mind, their
280 optical stability was tested by exposure to a light source of a dedicated laparoscopic fluorescence
281 camera ($\lambda_{\text{ex}} = 590\text{--}680$ nm). With the exclusion of ambient light, fluorophore solutions of 1 μM in PBS
282 were irradiated for a duration of 30 minutes, with an assessment of their fluorescence intensity at 5-
283 minute intervals. For most compounds, more than 90% of fluorescent signal remained after 30
284 minutes, indicating good optical stability (Figure 5A). Only compound **2** showed 30% photobleaching.
285 Although subtle, it is interesting to note that the fluorophores without sulfonates on the aromatic
286 rings portrayed a slightly lower photostability (**3–5**)(~ 88% remaining fluorescence intensity)
287 compared to the dyes with a sulfonated side chain (**6–11**)(95% remaining fluorescence intensity).
288 This indicates that the substitution of sulfonates on the aromatic rings positively affects the optical
289 stability of the fluorophores.

290 Earlier studies have underlined that it is also important that the dyes are chemically stable in
291 an *in vivo* environment [8,35]. To evaluate the chemical stability of the dyes towards endogenous

292 nucleophiles, they were incubated for up to 6 hours at 37 °C in a model buffer containing 0.5 mM
 293 glutathione [8,36]. UPLC-MS was used to discriminate if any adducts were formed by reaction with
 294 the respective thiol. As apparent from Figure 5B, all fluorophores remained stable and fluorescent at
 295 the given conditions. This finding excludes the formation of unwanted products during *in vivo*
 296 administration, as was previously reported for the NIR dyes ZW800-1 and IRdye 800-CW [8].
 297



298

299 **Figure 5.** Optical and chemical stability of the fluorophores and their tendency to interact with serum proteins.
 300 A) Optical stability; the dyes were illuminated using the light source of a prototype Karl Storz camera setup (λ_{ex}
 301 = 590–680 nm). Reduction in fluorescence was measured up to 30 min with 5-minute intervals. In the legend
 302 the dyes are given in order of decreasing stability (arrow). B) Chemical stability of the eleven dyes in 0.5 mM
 303 glutathione in HEPES (pH 7.4) at 37 °C as assayed overtime by UPLC-MS. C) Percentage of fluorophore bound
 304 to serum proteins after 18 h of dialysis with serum versus PBS. The fluorophores are grouped in colour by their
 305 alkyl substituents and within each group the dye with non-, one-, and two sulfonates on the aromatic ring are
 306 given from left to right.
 307

308 **3.4 Serum protein interaction**

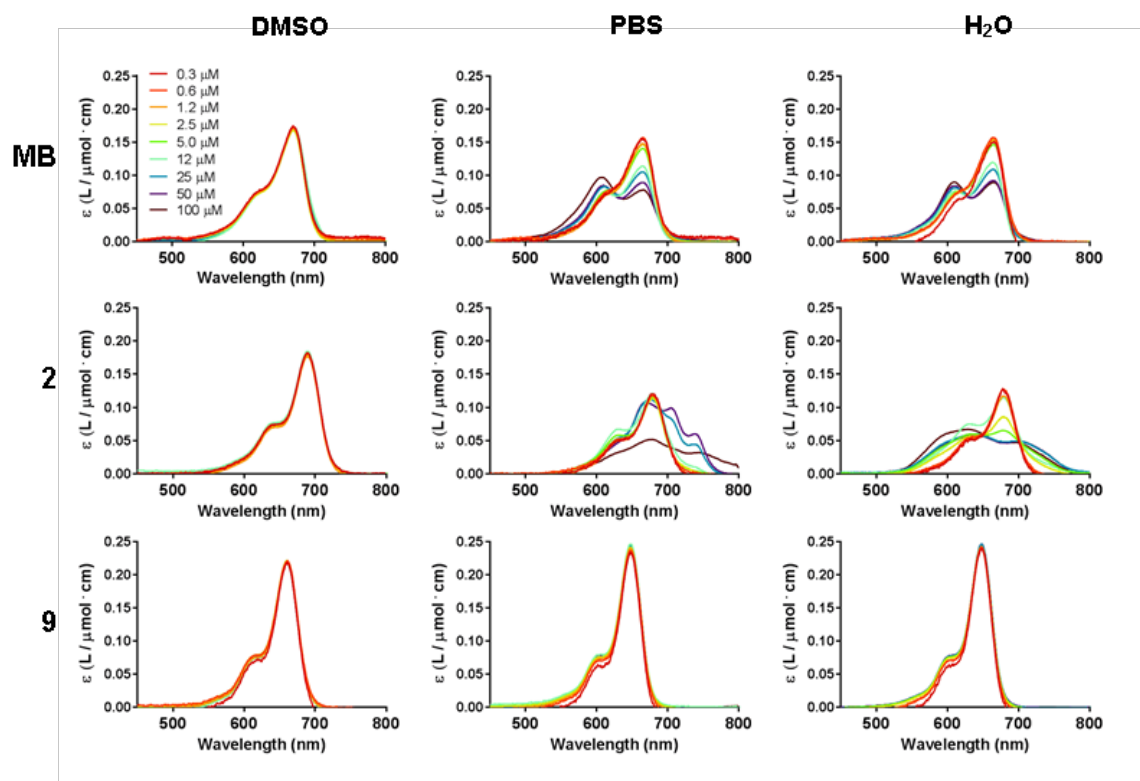
309 Next to the stability of the fluorophores towards endogenous nucleophiles, the tendency of the dyes
310 to non-covalently bind to serum proteins was also evaluated. Equilibrium dialysis against serum (18
311 h) revealed clear differences between the dyes (Figure 5C). Increasing the number of sulfonates on
312 the aromatic ring induced an approximate 50% decrease in serum protein binding following each
313 sulfonate introduced. Introducing a sulfonate on the side chain reduced the albumin interaction with
314 about 30% compared to the neutral (Me-) substituted dyes. The quaternary-amine substituents
315 reduced this even further. When these findings were related to the cLog P values, it appeared that
316 there is a threshold value at cLog P = 0.8. For dyes portraying a cLog P above this value, *i.e.* lipophilic
317 dyes, a serum protein binding tendency of > 50% was observed (compound **2**, **3** and **4**). When the
318 cLog P value drops below 0.8, the influence of the lipophilicity seems to become less substantial and
319 the number of charges on the compounds started to play a role, with the lowest percentage of
320 binding found for compound **9** and **11** (< 10%, five total charges). Overall, both the aromatic
321 substituents and alkyl substituents play a prominent role in the interaction with serum proteins.

322

323 **3.5 Stacking behaviour**

324 Previously we found that the degree of dye stacking observed in the reaction mixture was
325 predictive for the amount of stacking of the dyes on the obtained conjugation products [8]. In
326 general, the presence of multiple (stacked) dyes on the final product reduces the brightness and
327 homogeneity of the sample. Therefore, the stacking-based aggregation rates of the eleven
328 compounds investigated were determined in DMSO, PBS and H₂O at concentrations ranging from 0.3
329 to 100 μM. Compounds **3–11** did not aggregate in these solvents (Figure 6, for further details see Ref
330 [22]), while **MB** and compound **2** did demonstrate distinct stacking in the aqueous media (Figure 6).
331 Compound **2** showed aggregation at concentrations higher than 2.5 μM in PBS and H₂O. A
332 comparable aggregation tendency was reported earlier for **ICG** [8]. Based on this, the observed
333 stacking at > 2.5 μM concentration in aqueous medium seems to be induced by the presence of the

334 two additional aromatic rings. **MB** showed an even stronger dimeric stacking tendency than
335 compound **2**, while the concentration dependency of this effect was comparable to that of
336 compound **2** (Figure 6)[24].



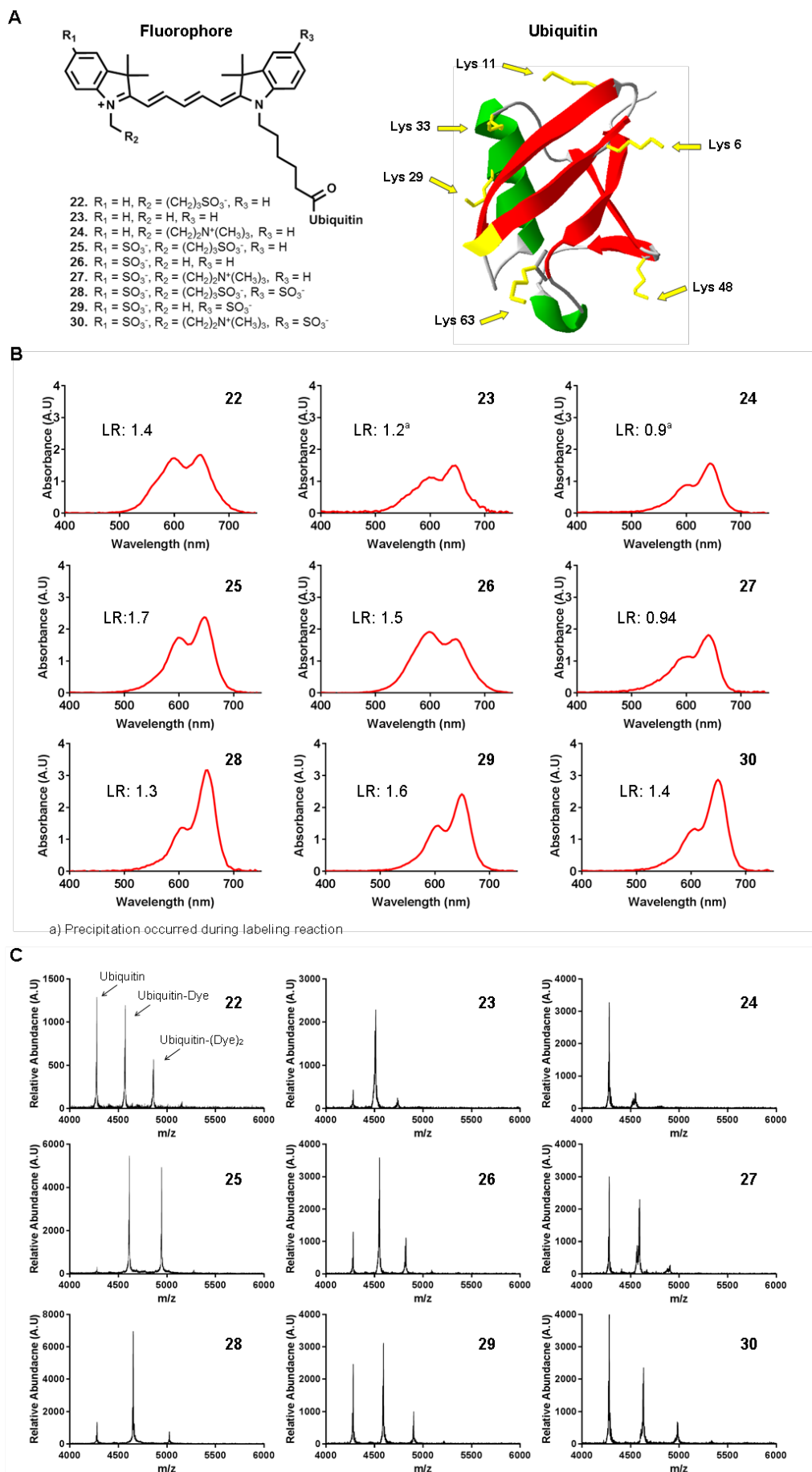
337
338 **Figure 6.** The stacking concentration dependency of **MB** and compound **2**, and **9** measured in DMSO, PBS and
339 H_2O at concentrations ranging from 0.3 to 100 μM . Compound **9** is shown as model for compound **3–11** as
340 they were all comparable. For detailed visualisation of each compound separately please refer to Ref [22].

341 342 3.5 Conjugation

343 To investigate if the structure variations in the fluorophores have an influence on their conjugation
344 characteristics, compounds **2–11** were activated (yielding compound **12–21**, see SI) and conjugated
345 to the reference protein Ubiquitin. This small (~ 8.5 kDa) [37], well-known regulatory protein is
346 present in almost every eukaryotic cell and contains 7 lysine residues of which 6 are solvent-exposed
347 (Figure 7A)(evaluated from the PDB structure 5DK8). The low molecular weight of Ubiquitin makes it
348 possible to study the labelling process *via* mass spectrometry (MS), which helps provide insight into

349 the homogeneity of the products obtained within a single sample. Relating these findings to the
350 absorbance profiles of the same products allowed for the determination of relative labelling ratios.

351 The labelling with the fluorophore **2** was unsuccessful due to its low solubility at the
352 required concentrations (100 μ M). Thus, the conjugation reactions yielded nine Ubiquitin constructs
353 (**22–30**). While previously no stacking was observed at the concentrations used in the reaction
354 mixture (Figure 6), absorption spectra of the conjugation products **22**, **23**, **25**, **26**, and **29** revealed
355 stacking (Figure 7B). The presence of sulfonate groups on the aromatic ring decreased the stacking
356 as did the presence of a quaternary amine on the side chain. When measured in DMSO, these
357 stacking interactions were no longer present due to increased solvation of the dyes (Figure S2) and
358 the dye loading rates could be accurately determined (Figure 7B; LR)[8]. The calculated loading rates
359 were found to be comparable (around 1) with exception of compounds **25** (1.7) and **29** (1.6).
360 However, except for being the only two dyes with a -2 net charge (Figure 3) there is no clear
361 indication why these loading rates were higher than the others.



363 **Figure 7.** A) The Cy5 dyes conjugated to Ubiquitin. Within the structure of Ubiquitin the surface-exposed lysine
364 groups and the N-terminus are indicated in yellow as probable binding sites for the fluorophores. The image
365 was constructed from the PDB structure 5DK8. B) Absorption spectra of the dyes conjugated to Ubiquitin (**22–**
366 **30**) measured in PBS, including the dye loading rates (LR). The fluorophores on construct **22, 23, 25, 26, and 29**
367 are stacking as is indicated by the increase of the right shoulder peak. The spectra are normalised on dye
368 concentration to underline the differences in the shape of the absorbances. C) Mass spectra of the conjugated
369 Cy5–Ubiquitin compounds. The mass signals of M^{2+} are shown as these were the most intense, with $m/z =$
370 4278 non-conjugated Ubiquitin, $m/z \approx 4500$ mono-conjugated Ubiquitin and $m/z \approx 4800$ di-conjugated
371 Ubiquitin.

372

373 When looking at the mass spectra of the conjugated Cy5-Ubiquitin compounds (**22–30**) it
374 becomes evident that the samples are heterogeneously labelled and that this effect differs between
375 dyes (Figure 7C). For the dyes with the sulfonated side chain (**22, 25, 28**), only the fluorophore with
376 two aromatic sulfonates (**28**) labelled homogeneously. For the dyes containing the methyl side chain
377 (**23, 26, 29**) however, lower number of sulfonates on the aromatic rings resulted in a more
378 homogeneously labelled Ubiquitin (**23**). MS analysis of the compounds with a quaternary amine on
379 the side chain (**24, 27, 30**) was more complex. The low ionisation of the mono or di-conjugated
380 Ubiquitin resulted in a discrepancy between the information obtained by MS and what was
381 calculated from the absorbance spectra. However, it can be concluded that also here the labelling
382 was heterogeneous as multiple peaks were visible. Combining the absorbance and MS data, we
383 demonstrated that while absorption spectra clearly indicate that the Cy5 dyes undergo a significant
384 degree of stacking (in PBS Figure 7B, not in DMSO; Figure S2), the same samples only displayed a
385 limited amount of di-conjugated Ubiquitin products (Figure 7C). Furthermore, no stacking was
386 observed for the free form of these compounds at the same concentration (Figure 4, Figure 3 in Ref
387 [22]). This suggests that the stacking observed is not the traditional dye–dye stacking, but comes
388 from stacking interactions with, *e.g.* tyrosine, tryptophan, or phenylalanine amino acids within the
389 protein. According to the crystal structure of Ubiquitin, there is at least one phenylalanine spatially

390 nearby every solvent-exposed Lysine (determined from the PDB structure 5DK8). The stacking
391 interaction with the surrounding amino-acids is also be noted by the quantum yield (Table 1). After
392 conjugation to the protein, the quantum yield of most compounds decreased, and the degree of
393 reduction correlated with the observed amount of stacking. Indeed, also the diminishing quantum
394 yield did not depend on whether the Ubiquitin is homogeneously labelled (one peak on the MS
395 data), thus underlining the fact that the observed stacking occurs between the dye and neighbouring
396 amino acids.

397 When the investigated dyes were compared in a biodistribution study with RGD it was found
398 that compound **7** yielded superior *in vivo* properties [17]. Based on the chemical characteristics
399 investigated herein however, compound **7** did not stand out, pointing out that chemical
400 characteristics are only one aspect in the development of efficient fluorescent tracers for *in vivo* use.
401 In the end, the Cy5 dye becomes but a component of a larger molecular structure, of which the
402 overall characteristics drive the targeting behaviour and biodistribution [17]. Given the apparent
403 balance that has to be obtained between the chemical characteristics of the dye and a targeting
404 vector, it seems to be inevitable that labelling of an individual targeting vector goes hand-in-hand
405 with screening of different Cy5-dyes structures, *e.g.* as presented in Figure 3. Nevertheless, in
406 fluorescent tracer design we would like to suggest that only dyes are used that are: (photo-
407)chemically stable, bright enough to obtain a signal-to-background ratio of at least 2 with the
408 cameras intended for clinical use, show no stacking in solution, and ideally label proteins
409 homogeneously.

410

411 **4. Conclusion**

412 In this study, the characteristic chemical and photophysical properties of ten systematically altered
413 Cy5 derivatives and their Ubiquitin conjugates were methodically analysed. Next to these structure–
414 activity relationships, the compatibility of the dyes with a clinical-grade fluorescence laparoscope
415 was also presented. Overall, the influence of the aromatic- and alkyl substituents on the chemical-

416 and photophysical properties of the ten Cy5 dyes has been documented more clearly, providing a
417 solid basis for future tracer developments.

418

419 **Acknowledgements**

420 The research leading to these results has received funding from the European Research Council
421 (ERC) under the European Union's Seventh Framework Program FP7/2007-2013 (Grant No. 2012-
422 306890), a Netherlands Organization for Scientific Research STW-VIDI grant (Grant No. STW
423 BGT11272). We thank KARL STORZ Endoskope GmbH & Co. KG for providing the prototype Cy5 light
424 source. We also like to thank A.R.P.M. Valentijn for making his lab available and providing the
425 Waters Acquity UPLC-MS system.

426

427 **References**

428 [1] Ferrari E, Gu C, Niranjana D, Restani L, Rasetti-Escargueil C, Obara I, et al. Synthetic self-
429 assembling clostridial chimera for modulation of sensory functions. *Bioconjug Chem*
430 2013;24:1750–9. doi:10.1021/bc4003103.

431 [2] van Leeuwen FWB, Hardwick JCH, van Erkel AR. Luminescence-based Imaging Approaches in
432 the Field of Interventional Molecular Imaging. *Radiology* 2015;276:12–29.
433 doi:10.1148/radiol.2015132698.

434 [3] Byrne WL, Delille A, Kuo C, de Jong JS, van Dam GM, Francis KP, et al. Use of optical imaging
435 to progress novel therapeutics to the clinic. *J Control Release* 2013;172:523–34.
436 doi:10.1016/j.jconrel.2013.05.004.

437 [4] van Leeuwen FWB, Valdés-Olmos R, Buckle T, Vidal-Sicart S. Hybrid surgical guidance based
438 on the integration of radionuclear and optical technologies. *Br J Radiol* 2016;89:20150797.
439 doi:10.1259/bjr.20150797.

440 [5] Yuan L, Lin W, Zheng K, He L, Huang W. Far-red to near infrared analyte-responsive
441 fluorescent probes based on organic fluorophore platforms for fluorescence imaging. *Chem*

- 442 Soc Rev 2013;42:622–61. doi:10.1039/c2cs35313j.
- 443 [6] Benson R., Kues HA. Fluorescence Properties of Indocyanine Green as Related to
444 Angiography. *Phys Med Biol* 1978;23:159–63.
- 445 [7] Azhdarinia A, Wilganowski N, Robinson H, Ghosh P, Kwon S, Lazard ZW, et al. Characterization
446 of chemical, radiochemical and optical properties of a dual-labeled MMP-9 targeting peptide.
447 *Bioorganic Med Chem* 2011;19:3769–76. doi:10.1016/j.bmc.2011.04.054.
- 448 [8] Van Der Wal S, Kuil J, Valentijn ARPM, Van Leeuwen FWB. Synthesis and systematic
449 evaluation of symmetric sulfonated centrally C-C bonded cyanine near-infrared dyes for
450 protein labelling. *Dye Pigment* 2016;132:7–19. doi:10.1016/j.dyepig.2016.03.054.
- 451 [9] Verbeek FPR, Vorst JR Van Der, Schaafsma BE, Swijnenburg R, Gaarenstroom KN, Elzevier HW,
452 et al. Intraoperative Near Infrared Fluorescence Guided Identification of the Ureters Using
453 Low Dose Methylene Blue : A First in Human Experience. *JURO* 2013;190:574–9.
454 doi:10.1016/j.juro.2013.02.3187.
- 455 [10] Hossam M, Askar SM. Minimally invasive , endoscopic assisted , parathyroidectomy (MIEAP)
456 with intraoperative methylene blue (MB) identification. *Egypt J Ear, Nose, Throat Allied Sci*
457 2012;13:25–30. doi:10.1016/j.ejenta.2012.02.003.
- 458 [11] Sari YS, Tunali V, Tomaoglu K, Karagöz B, İ AG, Karagöz İ. Can bile duct injuries be prevented?
459 “A new technique in laparoscopic cholecystectomy.” *BMC Surg* 2005;4:4–7.
460 doi:10.1186/1471-2482-5-14.
- 461 [12] FDA. Serious CNS reactions possible when methylene blue is given to patients taking certain
462 psychiatric medications 2011. <https://www.fda.gov/Drugs/DrugSafety/ucm263190.htm>.
- 463 [13] Mujumdar RB, Ernst L a, Mujumdar SR, Lewis CJ, Waggoner a S. Cyanine dye labeling
464 reagents: sulfoindocyanine succinimidyl esters. *Bioconjug Chem* 1993;4:105–11.
- 465 [14] Burggraaf J, Kamerling IMC, Gordon PB, Schrier L, Kam ML De, Kales AJ, et al. Technical
466 Reports Detection of colorectal polyps in humans using an intravenously administered
467 fluorescent peptide targeted against c-Met. *Nat Med* 2015;21. doi:10.1038/nm.3641.

- 468 [15] Phillips E, Penate-medina O, Zanzonico PB, Carvajal RD, Mohan P, Ye Y, et al. Clinical
469 translation of an ultrasmall inorganic optical-PET imaging nanoparticle probe. *Nanomedicine*
470 2014;6:1–9.
- 471 [16] Kuil J, Buckle T, Oldenburg J, Yuan H, Borowsky AD, Josephson L, et al. Hybrid peptide
472 dendrimers for imaging of chemokine receptor 4 (CXCR4) expression. *Mol Pharm*
473 2011;8:2444–53. doi:10.1021/mp200401p.
- 474 [17] Bunschoten A, van Willigen DM, Buckle T, van den Berg NS, Welling MM, Spa SJ, et al.
475 Tailoring Fluorescent Dyes To Optimize a Hybrid RGD-Tracer. *Bioconjug Chem* 2016;27:1253–
476 8. doi:10.1021/acs.bioconjchem.6b00093.
- 477 [18] Zhou Y, Kim Y, Milenic DE, Baidoo KE, Brechbiel MW. In Vitro and In Vivo Analysis of
478 Indocyanine Green-Labeled Panitumumab for Optical Imaging - A Cautionary Tale. *Bioconjug*
479 *Chem* 2014;25:1801–10. doi:10.1021/bc500312w.
- 480 [19] Bunschoten A, Buckle T, Kuil J, Luker GD, Luker KE, Nieweg OE, et al. Targeted non-covalent
481 self-assembled nanoparticles based on human serum albumin. *Biomaterials* 2012;33:867–75.
482 doi:10.1016/j.biomaterials.2011.10.005.
- 483 [20] Bunschoten A, Buckle T, Visser NL, Kuil J, Yuan H, Josephson L, et al. Multimodal
484 Interventional Molecular Imaging of Tumor Margins and Distant Metastases by Targeting
485 $\alpha\beta 3$ Integrin. *ChemBioChem* 2012;13:1039–45. doi:10.1002/cbic.201200034.
- 486 [21] Buckle T, Bunschoten A, Buckle T, Leeuwen AC Van, Chin PTK. A self-assembled multimodal
487 complex for combined pre- and intraoperative imaging. *Nanotechnology* 2010;21:1–9.
488 doi:10.1088/0957-4484/21/35/355101.
- 489 [22] Spa SJ, Hensbergen A, van der Wal S, Kuil J, van Leeuwen F. Data in Brief. *Data Br*
490 n.d.:Submitted.
- 491 [23] Pace CN, Vajdos F, Fee L, Grimsley G, Gray T. How To Measure and Predict the Molar
492 Absorption-Coefficient of a Protein. *Protein Sci* 1995;4:2411–23.
493 doi:10.1002/pro.5560041120.

- 494 [24] Bergmann K, O’Konski CT. a Spectroscopic Study of Methylene Blue Monomer, Dimer, and
495 Complexes With Montmorillonite. *J Phys Chem* 1963;67:2169–77. doi:10.1021/j100804a048.
- 496 [25] Morgounova E, Shao Q, Hackel BJ, Thomas DD, Ashkenazi S. Photoacoustic lifetime contrast
497 between methylene blue monomers and self-quenched dimers as a model for dual-labeled
498 activatable probes. *J Biomed Opt* 2013;18:56004. doi:10.1117/1.JBO.18.5.056004.
- 499 [26] Tredwell CJ, Keary CM. Picosecond time resolved fluorescence lifetimes of the polymethine
500 and related dyes. *Chem Phys* 1979;43:307–16. doi:10.1016/0301-0104(79)85199-X.
- 501 [27] Fisher NI, Hamer FM. A comparison of the absorption spectra of some typical symmetrical
502 cyanine dyes. *Proc Roy Soc* 1936:703–23. doi:10.1098/rspa.1983.0054.
- 503 [28] Chin PTK, Welling MM, Meskers SCJ, Valdes Olmos R a., Tanke H, van Leeuwen FWB. Optical
504 imaging as an expansion of nuclear medicine : Cerenkov-based luminescence vs fluorescence-
505 based luminescence 2013;40:1283–91. doi:10.1007/s00259-013-2408-9.
- 506 [29] Buckle T, Chin PTK, van den Berg NS, Loo CE, Koops W, Gilhuijs KG a, et al. Tumor bracketing
507 and safety margin estimation using multimodal marker seeds: a proof of concept. *J Biomed*
508 *Opt* 2012;15:56021. doi:10.1117/1.3503955.
- 509 [30] Yeung TM, Volpi D, Tullis IDC, Nicholson G a., Buchs N, Cunningham C, et al. Identifying
510 Ureters In Situ Under Fluorescence During Laparoscopic and Open Colorectal Surgery. *Ann*
511 *Surg* 2016;263:e1–2. doi:10.1097/SLA.0000000000001513.
- 512 [31] Mader O, Reiner K, Egelhaaf HJ, Fischer R, Brock R. Structure Property Analysis of
513 Pentamethine Indocyanine Dyes: Identification of a New Dye for Life Science Applications.
514 *Bioconjug Chem* 2004;15:70–8. doi:10.1021/bc034191h.
- 515 [32] Levitus M, Ranjit S. Cyanine dyes in biophysical research: the photophysics of polymethine
516 fluorescent dyes in biomolecular environments. *Q Rev Biophys* 2011;44:123–51.
517 doi:10.1017/S0033583510000247.
- 518 [33] Netzel TL, Nafisi K, Zhao M, Lenhard JR, Johnson I. Base-Content Dependence of Emission
519 Enhancements, Quantum Yields, and Lifetimes for Cyanine Dyes Bound to Double-Strand

520 DNA: Photophysical Properties of Monomeric and Bichromophoric DNA Stains. *J Phys Chem*
521 1995;99:17936–47. doi:0022-365419512099-17936.

522 [34] Schobel U, Egelhaaf H, Frohlich D, Brecht A, Oelkrug D, Gauglitz G. Mechanisms of
523 Fluorescence Quenching in Donor – Acceptor Labeled Antibody – Antigen Conjugates. *J*
524 *Fluoresc* 2000;10:147–54. doi:10.1023/A:1009443125878.

525 [35] Cilliers C, Nessler I, Christodolu N, Thurber GM. Tracking Antibody Distribution with Near-
526 Infrared Fluorescent Dyes: Impact of Dye Structure and Degree of Labeling on Plasma
527 Clearance. *Mol Pharm* 2017:acs.molpharmaceut.6b01091.
528 doi:10.1021/acs.molpharmaceut.6b01091.

529 [36] Costa CM da, Santos RCC dos, Lima ES. A simple automated procedure for thiol measurement
530 in human serum samples. *J Bras Patol E Med Lab* 2006;42. doi:10.1590/S1676-
531 24442006000500006.

532 [37] Goldstein G, Scheid M, Hammerling U, Schlesinger DH, Niall HD, Boyse EA. Isolation of a
533 polypeptide that has lymphocyte-differentiating properties and is probably represented
534 universally in living cells. *Proc Natl Acad Sci U S A* 1975;72:11–5. doi:10.1073/pnas.72.1.11.

535